

Suppressed reflectivity due to spin-controlled localization in a magnetic semiconductor.

F.P. Mena^{1,7}, J.F. DiTusa², D. van der Marel^{3,1}, G. Aeppli⁴, D.P. Young², A. Damascelli⁵, J.A. Mydosh⁶

¹*Materials Science Centre, University of Groningen, The Netherlands*

²*Department of Physics and Astronomy, Louisiana State University, USA*

³*Département de Physique de la Matière Condensée, Université de Genève, Switzerland*

⁴*London Centre for Nanotechnology, University College London, UK*

⁵*Department of Physics & Astronomy, University of British Columbia, Vancouver, Canada and*

⁶*II. Physikalisches Institut, Universität zu Köln, Germany*

⁷*Current Address: Space Research Organization of the Netherlands, Groningen, The Netherlands*

(Dated: November 17, 2018)

The narrow gap semiconductor FeSi owes its strong paramagnetism to electron-correlation effects. Partial Co substitution for Fe produces a spin-polarized doped semiconductor. The spin-polarization causes suppression of the metallic reflectivity and increased scattering of charge carriers, in contrast to what happens in other magnetic semiconductors, where magnetic order reduces the scattering. The loss of metallicity continues progressively even into the fully polarized state, and entails as much as a 25% reduction in average mean-free path. We attribute the observed effect to a deepening of the potential wells presented by the randomly distributed Co atoms to the majority spin carriers. This mechanism inverts the sequence of steps for dealing with disorder and interactions from that in the classic Al'tshuler Aronov approach - where disorder amplifies the Coulomb interaction between carriers - in that here, the Coulomb interaction leads to spin polarization which in turn amplifies the disorder-induced scattering.

I. INTRODUCTION

Future technologies based on the control and state of electron spins rather than charges are commonly referred to as spintronics. Efforts to produce materials for spintronics have mostly focused on thin film III-V semiconductors alloyed with manganese^{1,2,3,4}. In (Ga,Mn)As, the most fully characterized of these alloys, Mn substitutes a trivalent Ga ion and acts as a shallow acceptor just above the valence band. The Mn²⁺ impurities have a local moment associated with a high spin (S=5/2) configuration, and are ferromagnetically coupled below the Curie temperature (T_C) by a small number of itinerant hole carriers. In metallic and ferromagnetic (Ga,Mn)As these doped holes are thought to reside in an itinerant Mn-derived impurity band^{5,6} about 0.1 eV above the valence band.

Another route to magnetic semiconductors relies on carrier doping into narrow band, strongly correlated insulators. Perhaps the most celebrated is the monosilicide FeSi, which has been investigated for several decades because it has a large 300 K response to magnetic fields that vanishes as T approaches zero^{7,8,9,10,11}. Together with CoSi and the unusual metal MnSi^{12,13}, FeSi belongs to the larger group of transition metal monosilicides, allowing chemical substitutions across the entire series without change in the cubic B-20 crystal structure or the nucleation of second phases^{7,9}. Bulk single crystals can be grown and FeSi can be made metallic and ferromagnetic by the substitution of Co to form the silicon-based magnetic semiconductor Fe_{1-y}Co_ySi^{7,9}. Because the metals that result are disordered, quantum interference and electron-electron interactions were found to dominate the temperature and magnetic field dependent DC carrier

transport⁷. Given that optical properties are a key to potential spintronic applications¹⁴ and have been predicted, but not yet observed, to be sensitive to these interaction effects^{15,16,17}, we have measured the optical reflectivity $R(\omega)$ of Fe_{1-y}Co_ySi. Here we present the experimental manifestation of spin-polarization controlled localization on $R(\omega)$ and the optical conductivity $\sigma(\omega)$ of this magnetic semiconductor.

Before presenting the data, we describe what is expected in the three cases of undoped and doped semiconductors, and the simple magnetic metals formed from doped semiconductors. For clean semiconductors, the low-temperature optical conductivity is dominated by excitations across a gap between valence and conduction bands. Warming produces holes in the valence band as well as electrons in the conduction band, adding a Drude-peak centered at zero energy to the interband transitions. Chemical doping (Fig. 1a) adds carriers to the valence, conduction, or impurity bands and yields a zero-temperature $\sigma(\omega)$ which is very similar to that obtained by warming in the undoped case - the dominant low-energy feature is a Drude peak with weight proportional to the carrier density (n) and width $1/\tau$ measuring the scattering rate of the carriers. If the carriers were spin polarized, either via application of an external magnetic field or an internal exchange splitting from spontaneous magnetic order, their band would be split into majority and minority spin-bands as in Fig. 1b. Eventually the minority band can be shifted above the Fermi energy (E_F) resulting in a redistribution of all the carriers into the majority band. The outcome is called a half metallic ferromagnet¹⁸ (Figs. 1b and 1d), because electrons carrying the majority spin belong to a partially filled, metallic band, while those carrying the minority

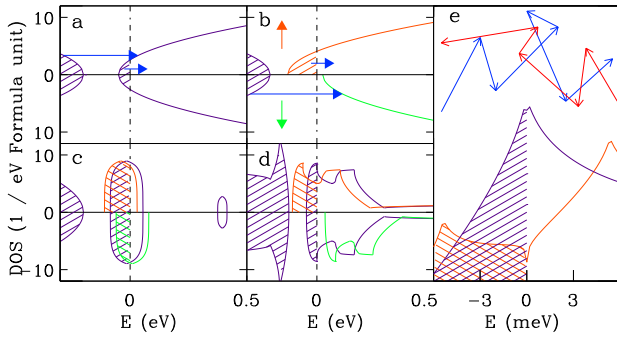


FIG. 1: Schematic density of states (DOS) for the up and down spin states of semiconductors, ferromagnetic semiconductors, and ferromagnetic metals. Blue arrows depict optically allowed interband transitions: (a) electron doped semiconductor, (b) fully spin-polarized doped semiconductor, (c) doped semiconductor where the added carriers reside in an impurity band within the band gap such as is thought to be the case for (Ga,Mn)As, (d) fully spinpolarized $\text{Fe}_{0.8}\text{Co}_{0.2}\text{Si}$. (e) Disordered conductor where increased Coulomb interactions lead to an enhanced DOS in the paramagnetic state (purple curve) and a singular, depleted DOS at E_F for the spin-polarized state (orange curve). The red and the blue lines at the top of the figure represent a diffusive path for two carriers in a disordered metal. Each crossing represents an interaction event, indicating multiple electron-electron scattering of the same two carriers without breaking quantum coherence.

spin belong to an empty (at $T = 0$) conduction band. To accommodate all of the itinerant electrons E_F shifts upward, decreasing the density of states (DOS) at E_F by a factor of $2^{2/3}$. Naively one might expect this reduction in the DOS to reduce the low-frequency $\sigma(\omega)$. However, the optical sum rule states that the integral of $\sigma(\omega)$ over ω measures the carrier density n , so that conservation of n in the parabolic band leads to conservation of $\sigma(\omega)$ through the phase transition as long the effective mass of the carriers does not change.

This is precisely what has been observed in previous measurements of spin polarized metals such as CrO_2 and NiMnSb , where the only consequence of the half-metallicity is a slight increase in the scattering rate at energies above that required to transfer a carrier between the majority and the unoccupied minority bands^{19,20}. Similarly, measurements of $\sigma(\omega)$ of the magnetic semiconductor (Ga,Mn)As reveal changes to the spectrum below T_C due to a reduction of τ^{-1} and m^* ^{5,6}. As a result $\sigma(\omega)$ increases at ω below 350 meV, causing an increase of the reflectivity, or, in other words, a *positive* magnetic-order-induced reflectivity. Perhaps the most impressive increases in reflectivity at a ferromagnetic transition occur in the optical spectra of EuB_6 and $\text{La}_{1-x}\text{Sr}_x\text{MnO}_3$ ^{21,22}. In these cases cooling into the FM state is accompanied by large increases in the Drude spectral weight due to concurrent semimetal- or insulator-metal transitions.

II. EXPERIMENTAL METHODS

Single crystals were grown from high purity starting materials (99.995% or greater) by either vapor transport, light image furnace floating zone, or modified tri-arc Czochralski methods. X-ray spectra showed all samples to be single phase with a lattice constant linearly dependent on y demonstrating that Co successfully replaces Fe over the entire concentration range ($0 \leq y \leq 1$). Energy dispersive X-ray microanalysis yielded results consistent with the nominal concentrations.

The reflectivity of these single crystals was measured from 4 meV to 0.75 eV while ellipsometry was used to measure directly the dielectric function from 0.74 to 4.5 eV. In order to monitor in detail the change of reflectivity as a function of temperature reported in this manuscript and in a number of other recent experiments of the same laboratory^{23,24,25}, typical standard optical tail cryostats which are commercially available can not be used. The precision and stability needed in this work requires a sampling of infrared and optical spectra with a very dense interval of temperatures, and an overall system stability on the order of 0.1 % of the reflected signal or better. We use special design optical cryostats, which differ from commercial designs in several important aspects. Further details are described in Ref. 26.

Between 4 and 750 meV we used Kramers-Kronig relations, along with a Hagen-Rubens extrapolation of $R(\omega)$ data to $\omega = 0$, to obtain the phase of $R(\omega)$, and subsequently $\epsilon(\omega)$. $\sigma(\omega)$ is obtained via the relation $\text{Re}\sigma = (\omega/4\pi)\text{Im}\epsilon(\omega)$. We have carefully checked that $\sigma(\omega)$ is not significantly altered by our choice of high- and low- ω terminations. The Kramers-Kronig output was locked to the ellipsometrically measured $\epsilon_1(\omega)$ and $\epsilon_2(\omega)$, which strongly improves the accuracy. The optical reflectivity at low frequencies and the optical conductivity obtained from the Kramers-Kroning analysis proved to be consistent with the experimental DC resistivity.

III. OPTICAL REFLECTIVITY

$\text{Fe}_{1-x}\text{Co}_x\text{Si}$ spans insulating, metallic and polarized metallic regimes, and is interesting and important because on the Fe-rich side of the phase diagram⁷, it defies the standard expectations for all three. In Fig. 2 we compare the reflectivity spectra at 10 K of $\text{FeSi}, \text{CoSi}, \text{MnSi}$ and $\text{Fe}_{1-x}\text{Co}_x\text{Si}$ with $x=0.1, 0.2, 0.3$. The latter three samples order magnetically at $T_C = 10, 36$ and 49 K, while MnSi orders at 29.5 K^{7,27}. All samples shown except FeSi become 100 % reflecting in the limit $\omega \rightarrow 0$, as expected because they are good electrically conducting materials. The reflectivity spectra reveal optical phonons at approximately 25, 40, 43 and 56 meV, the shape of which vary progressively from the asymmetric dispersive variety for the semiconducting samples to negative dips for the more metallic samples. This is a direct manifestation of the negative term contributed to the dielectric

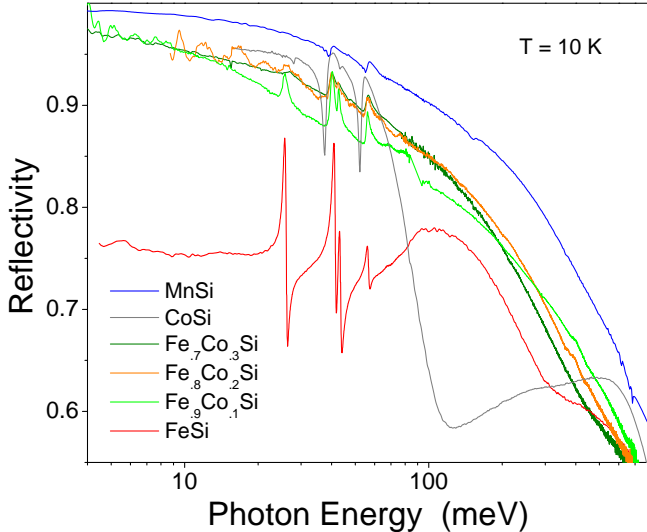


FIG. 2: Normal incidence reflectivity spectra of FeSi, CoSi, $Fe_{1-x}Co_xSi$, and MnSi measured at 10 K.

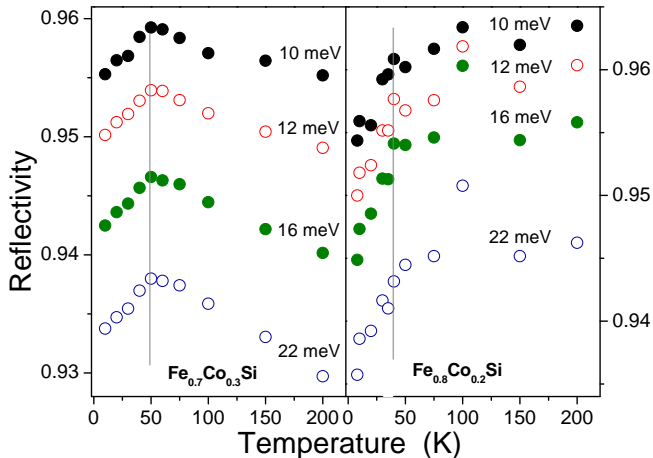


FIG. 3: Temperature dependence of the reflection coefficient of $Fe_{0.8}Co_{0.2}Si$ and $Fe_{0.7}Co_{0.3}Si$ for four different infrared photon energies. The vertical gray lines indicate the corresponding magnetic ordering temperature.

function by the free charge carriers, in addition to the optical phonon oscillators. MnSi is a relatively good metal at these temperatures, causing the strong screening of the optical phonons in the reflectivity spectra. In an earlier publication the infrared reflectivity of MnSi has been reported to increase when it becomes magnetically ordered¹². This is a natural consequence of the suppression of the spin-disorder scattering of the electrons, simultaneously suppressing the scattering rate of the free charge carriers and increasing the amplitude of the low frequency dielectric constant.

The central experimental result of this paper is the temperature dependence of the reflectivity of $Fe_{1-x}Co_xSi$, shown in Fig. 3. The different behaviour of the paramagnetic state also exists for the transport properties, and it reflects the closer proximity to the

metal insulator transition of samples with a smaller carrier concentration. Both $Fe_{0.8}Co_{0.2}Si$ and $Fe_{0.7}Co_{0.3}Si$ behave exactly opposite to MnSi when the magnetic order occurs: The reflectivity of both samples is clearly suppressed in the ordered state, *i.e.* in the magnetically ordered phase the material becomes less metallic as compared to the paramagnetic phase. We observed no spin-ordering induced change of reflectivity in the 10 % doped sample, which is not surprising: T_C of this sample is 10 K. Assuming that the spin-ordering induced changes are similar to those of the other two samples, the estimated change of reflectivity between 6 Kelvin (the lower limit of this cryostat) and 10 Kelvin is only about 0.0005, which is too small to detect with the current accuracy.

IV. OPTICAL CONDUCTIVITY

In order to obtain a clear experimental picture of this effect, we examine the optical conductivity spectra for a few selected temperatures, shown in Fig. 4 for the semiconducting parent compound FeSi, and $Fe_{1-x}Co_xSi$. We begin with pure CoSi (top frames in Fig. 4), long known as a diamagnetic metal with a very low carrier density, $\sim 1\%$ of electrons/formula unit²⁸. Our data agree with the simple ideas outlined above; *i.e.* there is a small Drude peak centered at $\omega = 0$ which coexists with interband transitions beginning at ~ 125 meV. At $T = 10$ K, the width of the Drude peak is $\hbar/\tau = 20$ meV, which in the simplest analysis implies a carrier mean free path of 5 nm. The main effect of warming to 300 K is to broaden the Drude peak by an amount less than $k_B T$.

The lower frame of Fig. 4 displays data for the alloy's other end member, insulating FeSi. The optical conductivity, which shows no hint of a band gap at 300 K, is almost completely suppressed below 75 meV upon cooling to 10 K, as in Ref. 29 which emphasized that in a conventional band picture, remnants of a 60 meV gap should be clearly visible at 300 K (26 meV). This disappearance of the semiconductor gap at approximately 200 K has been confirmed by subsequent investigations of the optical properties^{30,31}. A second important feature is that the energy range over which $\sigma(\omega)$ changes as a function of temperature, is extremely large as indicated by the logarithmic ω scale in Fig. 4. Careful analysis of the temperature dependence of the integrated spectral weight³⁸ confirms the result of Ref. 29, that there is a lack of spectral weight conservation to energies above 80 times E_g . Even if the spectral weight would be distributed over a wide spectral range in an unmeasurable way, it is not recovered on the energy scale of a few times the gap as expected.

While the obliteration of all remnants of a 60 meV gap at 300 K can be attributed, at least in part, to the feedback of vibrational disorder on the electronic structure using a conventional band picture where electron-electron correlations are treated within the framework of the Local Density Approximation³², the issue of the

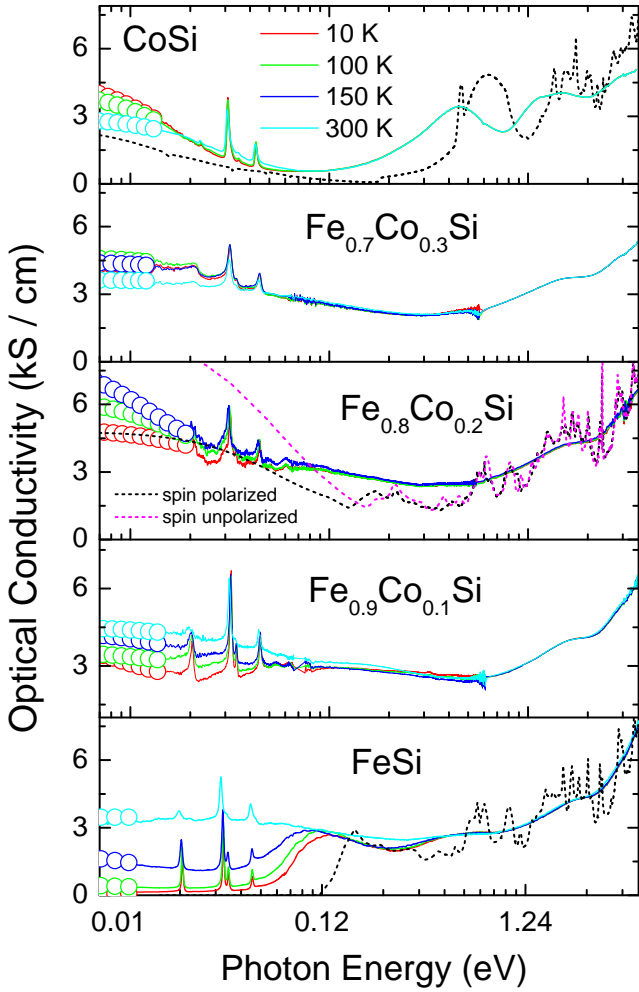


FIG. 4: Experimental optical conductivity spectra of $\text{Fe}_{1-x}\text{Co}_x\text{Si}$ for $x=0.0, 0.1, 0.2, 0.3$ and 1.0 . (solid lines and open circles). The calculated optical conductivity using the Local Density Approximation is shown for FeSi , $\text{Fe}_{0.8}\text{Co}_{0.2}\text{Si}$ and CoSi (olive dashed curves). Widths (τ^{-1}) of the Drude peaks were chosen to minimize the deviation from the experiment spectra. For $\text{Fe}_{0.8}\text{Co}_{0.2}\text{Si}$, the calculation corresponding to full spin-polarization (purple dashed curves) is a much better estimate for the Drude weight than unpolarized calculation (olive dashed curve), even at 300 K, consistent with short range magnetic order well above T_C .

spectral weight redistribution appears to require a more rigorous treatment of the correlation effects. Urasaki and Sasai³³ treated the bands on either side of the gap with the 2-band Hubbard model, while assuming a moderate U ($U = 0.5$ eV). Their calculated optical spectra agree in detail with the experiments. In particular their model explains both the temperature shift of gap edge, and the temperature dependent spectral weight redistribution. Taken together this suggests the important role of electron-correlations for the physical properties of FeSi ^{33,34,35,36}.

Doping FeSi via substitution of Co for Fe yields similar problems for the standard model underlying semi-

conductor optics. The conductivity of the 10 percent doped sample exhibits a suppression below 10 meV for $T < 50$ K, but there is no complete gap like in FeSi at the same temperatures. In contrast to the data for pure CoSi , but in agreement with our findings for FeSi at 300 K, $\text{Fe}_{1-x}\text{Co}_x\text{Si}$ for the three dopings considered here displays a $\sigma(\omega)$ which decays weakly from $\hbar\omega = 0$ to 350 meV, while all traces of the gap in the pure FeSi parent are obliterated³⁷. Even with the assumption of a scattering rate in excess of the 60 meV gap of FeSi , a simple Drude analysis (dashed lines in Fig.4) based on our band structure calculations cannot account for $\sigma(\omega)$. We conclude that treating the electrons in $\text{Fe}_{1-y}\text{Co}_y\text{Si}$ as a simple Fermi liquid formed in the conduction band is incorrect, notwithstanding the remarkable simplicity of aggregate $\omega = 0$ properties such as the normal Hall effect and ordered magnetization, which correspond to one carrier and one polarized spin per Co atom⁷.

Beyond showing that the parent insulator and its electron-doped derivative violate standard ideas about undoped and doped semiconductors, Fig.4 also reveals that $\text{Fe}_{1-y}\text{Co}_y\text{Si}$ defies expectations for itinerant magnets. In particular, cooling yields a suppression of the low-frequency conductivity of a different qualitative nature than seen for FeSi , where it occurs throughout the gapped region. The suppression of the optical conductivity is of course consistent with the suppression of the dc conductivity from the dc transport measurements, as well as the raw reflectivity data $R(\omega)$ of Fig. 3. Thus, in contrast to what occurs for all other metallic ferromagnets, including MnSi ³⁸ and $(\text{Ga},\text{Mn})\text{As}$ ^{5,6}, the approach and onset of magnetic order at $T_C = 36$ K decreases the conductivity and suppresses the metallic screening of $\text{Fe}_{1-y}\text{Co}_y\text{Si}$.

Figure 5 reveals more detail on the evolution of the optical data with T , and compares them to transport and magnetization data. $R(\omega)$ in Fig.3 at low ω simply follows the $\sigma(\omega = 0)$ (Fig. 5), which experiences its main drop below T_C . For higher ω (not shown), $R(\omega)$ decreases continuously from 300 K, with no visible anomaly at T_C for photon energies larger than 40 meV. The obliteration of singular behaviour near T_C with increasing ω is in accord with the extended critical regime, or superparamagnetism (field induced short range order), indicated by the magnetization data of Fig.5d. Here a modest (compared to $k_B T$) external field of 5 T produces very appreciable polarization to T 's as high as $100\text{ K} \sim 3T_C$. Fig.5f shows $\sigma(\omega, T)$ of $\text{Fe}_{0.8}\text{Co}_{0.2}\text{Si}$ after subtraction of $\sigma(\omega)$ of FeSi , revealing where the added carriers reside in the excitation spectrum of the nominally pure compound. Cooling builds up the differential (relative to the insulator) spectral weight down to T_C , whereupon there is a loss especially apparent below 25 meV. Again, our observation of a reduced spectral weight below T_C contradicts both the standard models based on independent quasiparticles and measurements for other magnetic semiconductors^{5,6}.

In addition, cooling below T_C causes the wide Drude-like peak to broaden, rather than to narrow. We have

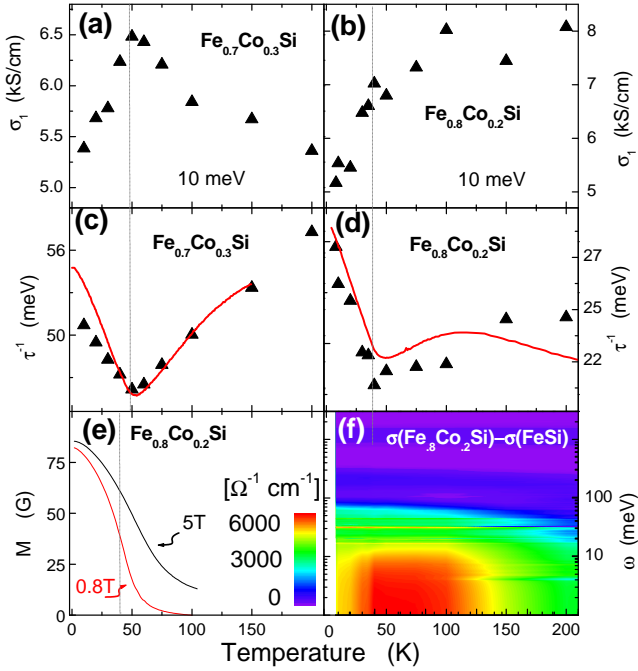


FIG. 5: Temperature dependence of related physical properties of $\text{Fe}_{1-x}\text{Co}_x\text{Si}$ for two different doping concentrations. The optical conductivity $\sigma(\omega)$ for $\hbar\omega = 10$ meV (a and b), the corresponding optical scattering rates \hbar/τ (triangles in c and d), DC resistivities scaled as to overlay the scattering rates (red solid curves in c and d), bulk magnetization of $\text{Fe}_{0.8}\text{Co}_{0.2}\text{Si}$ (e), and optical conductivity difference of $\text{Fe}_{0.8}\text{Co}_{0.2}\text{Si}$ and FeSi for a large range of temperatures and frequencies f. The corresponding magnetic ordering temperatures are indicated by the grey lines.

parameterized the low- ω $\sigma(\omega)$ by fitting the standard Drude form, superposed on a T -independent Lorentzian peak at 800 cm^{-1} , to the data. Fig.5 displays the resulting scattering rates (τ^{-1}), which track the bulk resistivities ($1/\sigma_1(\omega = 0)$) and undergo a sharp upturn below T_C . The important and unique contribution of the optical data is to show that the unusual rise in resistivity below T_C is due to enhanced scattering as opposed to a reduction of the charge carrier density/mass ratio.

V. DISCUSSION

To begin to understand our data, we have calculated the density of states (Fig.6) as well as $\sigma(\omega)$ (Fig.4) derived from the band structure of $\text{Fe}_{1-y}\text{Co}_y\text{Si}$. These calculations employ the Local Density Approximation (LDA) with the Gunnarsson-Lundquist exchange correlation potential carried out self consistently using the full potential linear muffin-tin orbital method^{44,45,46}. For $\text{Fe}_{0.8}\text{Co}_{0.2}\text{Si}$ a non-integer charge to iron in FeSi was assigned. We evaluated $\sigma(\omega)$ with a k-space integration over 216 points in the irreducible part of the Brillouin zone³⁸. The band structure agrees with the magnetiza-

tion and Hall effect and more complicated supercell calculations, in that the minority spin Fermi surface resides in a gap^{7,8,39}. It also supports the picture that Co doping merely adds electrons to bands inherited from the FeSi parent, revealing, as does experiment, that CoSi (with one extra electron/Fe) is a very low n metal.

While treating electron-correlations within the framework of the LDA (Fig.6) has some successes (for example in explaining the ground state properties), for the description of the relevant (magneto-) transport and optical properties it is necessary to take into account the impact of electronic correlations on the excited states. Generally speaking this requires a treatment beyond the Local Density Approximation. Important experimental observations which need to be understood are the apparent loss of carriers at low- ω , and the increase—instead of the conventional decrease—in τ^{-1} below T_C of $\text{Fe}_{1-y}\text{Co}_y\text{Si}$. To make progress, the Coulomb interactions need to be considered. How these underpin the moment formation at modest T , as well as the rapid filling of the gap in the parent compound via the paradigm of the Kondo insulator, is discussed elsewhere^{33,34,35,36}.

Why do we observe an increased scattering rate below T_C , opposite in sign to Mn doped GaAs and MnSi? For weak spin-polarization, this effect most likely follows from the interplay of Coulomb coupling and the quantum mechanical interference of diffusing charge carriers^{15,16}. This feature of disordered metals, hitherto seen only in transport and tunneling, but witnessed optically for the first time in our experiments, is demonstrated schematically in Fig.1g. Arrows at the top of the figure demonstrate diffusive paths for two carriers in a disordered metal. The large elastic scattering rate results in multiple scattering of these same two carriers without breaking quantum coherence, effectively enhancing their Coulomb interaction because the carriers are visible to each other more often. The increased Coulomb coupling induces square-root singularities in the density of states at E_F ^{15,16}. Spin-polarization, either from external magnetic fields or a spontaneous magnetization, shifts the singularities with respect to E_F resulting in a reduction of $\sigma(\omega)$ ^{15,16}, illustrated schematically in the figure. Thus $\sigma(\omega)$ and $R(\omega)$ display singular behaviour in T at low- ω just as we observe. MnSi, the only other known magnet in the transition metal monosilicide group, is not a disordered metal, in accordance with our observation of no magnetic-order-induced reduction of the reflectivity³⁸. However, well below T_C the saturation magnetization of $\text{Fe}_{1-x}\text{Co}_x\text{Si}$ with $x < 0.3$ approaches⁷ that of a halfmetallic ferromagnet (Fig. 1d). In this limit one of two spin components is absent near the Fermi energy, a state of affairs quite distant from the situation considered in Fig.1g. As we will explain below, disorder and Coulomb interactions appear to control the optical and magnetotransport anomalies of these compounds also in the limit of strong spin-polarization.

The explanation here stems from the strong 3d-character of the conduction bands. In a tight binding

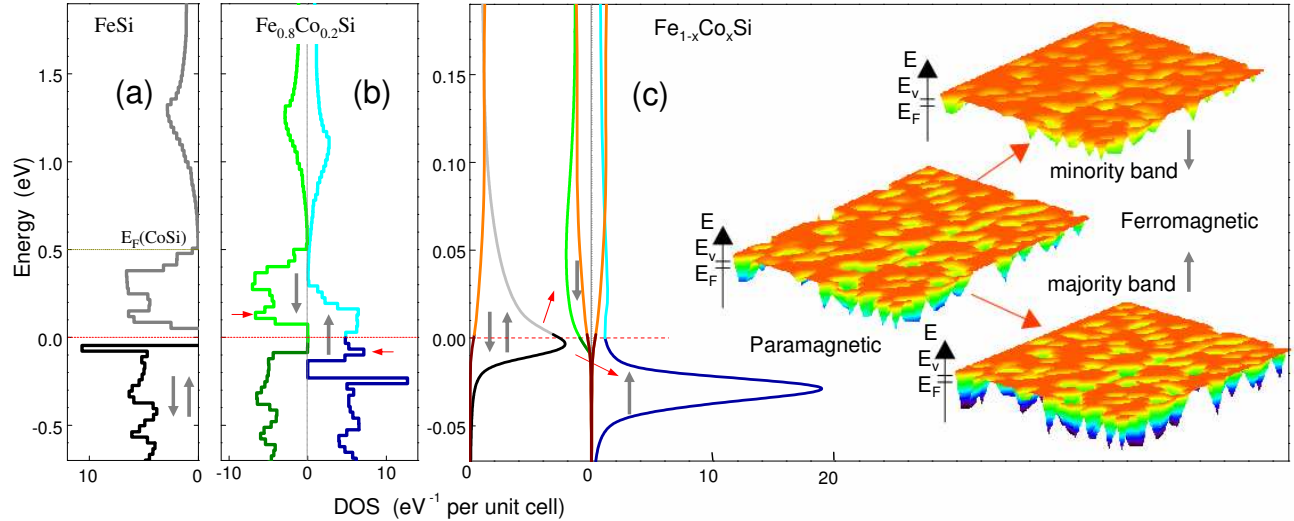


FIG. 6: (a) Calculated density of states of FeSi. The Fermi energy (red line) is inside the semiconductor gap. The band-calculations of CoSi give a very similar DOS, with the Fermi energy shifted to a higher energy (dark dotted line). (b) DOS of $\text{Fe}_{0.8}\text{Co}_{0.2}\text{Si}$ using the virtual crystal approximation³⁹. These results confirm the full spin polarization of $\text{Fe}_{0.8}\text{Co}_{0.2}\text{Si}$. Arrows indicate E_F in unpolarized state. (c) Local DOS at the Co atom substituting Fe in FeSi in the unpolarized state (grey curves) and the spin-polarized state (blue and green curves), calculated using the tight-binding Green's function formalism^{40,41}, while treating the on-site Hubbard repulsion in the mean field approximation^{42,43}. The orange curves are the DOS of the FeSi host material. The Fermi energy (E_F) lies just above the FeSi conduction band edge (E_c). The potential energy landscape for the carriers due to the Co impurities is sketched on the righthand side. In the ferromagnetic state carriers in the majority spin sub-band scatter more strongly from the random potential than either carriers in the minority spin sub-band or in paramagnetic bands due to the increased depth of the potential wells.

picture of $\text{Fe}_{1-x}\text{Co}_x\text{Si}$ the random substitution of Co for Fe within the FeSi lattice corresponds to deepening the potential-well of the Co-sites, allowing one extra electron per site to enter. This attractive potential causes a downward shift of the local DOS of the Co-atoms relative to the FeSi DOS. Provided that this potential exceeds a critical value, an impurity state will be pulled below the conduction band, *i.e.* inside the semiconductor gap. However, even if the potential is smaller than the critical value, the local DOS on the Co-sites has a pile-up of states near the gap (grey curves in Fig. 6c). In this scenario the elastic scattering of the conduction electrons is a consequence of the disordered potential landscape (Fig. 6c) and, in the case of $\text{Fe}_{1-x}\text{Co}_x\text{Si}$, brings the system close to an Anderson metal-insulator transition. How close is indicated by the product $k_F l$ of the Fermi vector and mean free path which we measure to be 6.9 if we assume a single Fermi surface, and 1.3 if we consider that there are 12 electron pockets⁴⁷. As this weakly metallic electron gas is cooled, the spin splitting of the bands due to the exchange interaction shifts the majority and minority bands of Co-3d character with respect to the FeSi conduction band. The consequence for the disordered potential landscape is illustrated in the right hand side of Fig. 6c where the depth of the potential wells in proximity to the Co-sites is increased (decreased) for the majority (minority) spin sub-band. Consequently, the majority spins are more strongly scattered compared

to the paramagnetic, or unpolarized high temperature, state. The net magnetoresistance of two parallel channels is⁴⁸ $\rho^{-1} = \rho_{\uparrow}^{-1} + \rho_{\downarrow}^{-1}$ where ρ_{σ} are the resistivities of each spin-channel separately, if spin flip scattering, such as arising from spin-orbit coupling, can be neglected. In the limit of vanishing spin-polarization the sign of the magnetoresistance depends on the microscopic details of the model describing ρ_{σ} as a function of doping⁴⁸. However, in the present case an almost fully spin-polarized state is observed at low temperatures, hence we consider here the limit where the spin-splitting of the energy levels is large. Due to hopping between the Co-sites the states inside the gap form bands, and at the high doping levels considered here the width of these bands is a considerable fraction of the bandwidth of FeSi. For moderate spin-splitting, these bands merge with the FeSi conduction band, and the DOS at E_F remains ungapped, and the density of states still resembles that given by the virtual crystal approximation³⁹ presented in Fig. 6b. Ultimately, for a sufficiently large spin-splitting the majority spin-states become separated from the conduction band by a gap. Since the number of doped electrons is exactly equal to the number of majority spin-states, the Fermi-level resides inside this gap. Consequently this state of matter is not only fully spin-polarized, but it is also an insulator. In other words, in the limit of large spin-polarization both ρ_{\uparrow} and ρ_{\downarrow} diverge, the former because all localized up-states are occupied, the latter because the

down-states are empty in this limit. While these extreme conditions appear not to be met in the case of Co-doped FeSi, the majority spins in this material do outnumber the minority spins by a large fraction below T_C , hence the dominant effect at high spin-polarization is a positive magneto-resistance, just as we observe in Fig. 5.

The Al'tshuler-Aronov description and the model outlined above both take elastic scattering and Coulomb interactions as the starting point, and both lead to the same conclusion, namely that spin-polarization of a disordered metal leads to enhanced scattering. Whereas the former captures the subtle low energy scale effects caused by the coherent scattering between impurities, the latter becomes relevant in the limit of strong local perturbing potentials and a high degree of spin-polarization. Actually, in our description, we consider first the effect of the Coulomb interaction as the cause of spin order and therefore, via exchange splitting of the bands, an amplifier of potential scattering, whereas Al'tshuler-Aronov considers disorder as source of scattering which then amplifies the Coulomb interaction. The unification of these two limiting cases in a single framework remains a theoretical challenge yet to be met, although we suspect that a two-parameter scaling description might eventually account for the remarkable success of the Al'tshuler-Aronov expressions in accounting for the magnetoconductance of FeCoSi over such a wide range of fields and temperature⁷.

The reason for the differences from $\sigma(\omega)$ of (GaMn)As now becomes clear; the bands with Mn d-character are well below the GaAs valence band and produce a local magnetic moment interacting with the conducting holes. Therefore the effect of polarization on the carrier elastic scattering is less important and only small changes to $\sigma(\omega)$ due to variations in the spin disorder scattering are

observed.

VI. CONCLUSIONS

We have shown that the optical properties of $\text{Fe}_{1-y}\text{Co}_y\text{Si}$ are very different from those for (Ga,Mn)As, even though bulk properties such as the off-diagonal conductivity are remarkably similar^{7,8}. Doping produces an optical response throughout the gap of FeSi, implying that we are dealing not with an impurity band as in (Ga,Mn)As—but rather with carriers donated to the conduction band of FeSi. Finally, we have discovered an optical reflectivity which decreases rather than increases upon entering the spin-polarized state. The corresponding rise in the scattering rate, uniquely visible in the optical data, demonstrates that the origin of this effect is the Coulomb interaction between electrons in a disordered system.

VII. ACKNOWLEDGEMENTS

This work was supported by the National Science Foundation under contract No. DMR0406140, a Wolfson-Royal Society Research Merit Award, the Basic Technologies program of the UK Research Councils, the Swiss National Science Foundation through the NCCR 'Materials with Novel Electronic Properties', and the Netherlands Foundation for Fundamental Research on Matter with financial aid from the Nederlandse Organisatie voor Wetenschappelijk Onderzoek. We gratefully acknowledge A. A. Menovsky, C. Presura and A.I. Poteryaev for their assistance with crystal growth, optical experiments and LDA calculations respectively.

¹ H. Ohno, H. Munekata, T. Penney, S. von Molnar, and L.L. Chang, Phys. Rev. Lett. **68**, 2664-2667 (1992).

² H. Ohno, A. Shen, F. Matsukura, A. Oiwa, A. Endo, S. Katsumoto, and Y. Iye, Appl. Phys. Lett. **69**, 363-365 (1996).

³ F. Matsukura, H. Ohno, A. Shen, and Y. Sugawara, Phys. Rev. B **57**, R2037-2040 (1998).

⁴ M.L. Reed, N.A. El-Masry, H.H. Stadelmaier, M.K. Ritums, M.J. Reed, C.A. Parker, J.C. Roberts, and S.M. Bedair, Appl. Phys. Lett. **79**, 3473-3475 (2001).

⁵ E.J. Singley, R. Kawakami, D.D. Awschalom, and D.N. Basov, Phys. Rev. Lett. **89**, 097203 1-4 (2002).

⁶ E.J. Singley, K.S. Burch, R. Kawakami, J. Stephens, D.D. Awschalom, and D.N. Basov, Phys. Rev. B **68**, 165204 1-14 (2003).

⁷ N. Manyala, Y. Sidis, J.F. DiTusa, G. Aeppli, D.P. Young, and Z. Fisk, Nature **404**, 581-584 (2000).

⁸ N. Manyala, Y. Sidis, J.F. DiTusa, G. Aeppli, D.P. Young, and Z. Fisk, Nature Materials **3**, 255-262 (2004).

⁹ J.H. Wernick, G.K. Wertheim, and R.C. Sherwood, Mat. Res. Bull. **7**, 1431-1441 (1972).

¹⁰ V. Jaccarino, G.K. Wertheim, J.H. Wernick, L.R. Walker, and S. Arajs, Phys. Rev. **160**, 476-482 (1967).

¹¹ G. Aeppli, and Z. Fisk, Comments Condens. Matter Phys. **16**, 155-165 (1992).

¹² F.P. Mena, D. van der Marel, A. Damascelli, M. Fäh, A.A. Menovsky, and J.A. Mydosh Phys. Rev. B **67**, 241101(R), (2003).

¹³ N. Doiron-Leyraud, I.R. Walker, L. Taillefer, M.J. Steiner, S.R. Julian, and G.G. Lonzarich, Nature **425**, 595-599 (2003).

¹⁴ S.A. Wolf, D.D. Awschalom, R.A. Buhrman, J. M. Daughton, S. von Molnár, M.L. Roukes, A.Y. Chtchelkina, and D.M. Treger Science **294**, 1488-1495 (2001).

¹⁵ B.L. Al'tshuler, A.G. Aronov, M.G. Gershenson, and Yu. V. Sharvin, Sov. Sci. Rev. A Phys. **9**, 223-354 (1987).

¹⁶ P.A. Lee, and T.V. Ramakrishnan, Rev. Mod. Phys. **57**, 287-337 (1985).

¹⁷ A.J. Millis, and P.A. Lee, Phys. Rev. B **30**, 6170 (1984); erratum **31**, 5523-5524 (1985).

¹⁸ R.A. de Groot, F.M. Mueller, P.G. van Engen, and K.H.J. Buschow, Phys. Rev. Lett. **50**, 2024-2027 (1983).

¹⁹ E.J. Singley, C.P. Weber, D.N. Basov, A. Barry, and J.M.D. Coey, Phys. Rev. B **60**, 4126-4130 (1999).

²⁰ F.B. Mancoff, B.M. Clemens, E.J. Singley, and D.N. Basov, Phys. Rev. B **60**, R12565 (1999).

²¹ L. Degiorgi, E. Felder, H.R. Ott, J.L. Sarrao, and Z. Fisk, Phys. Rev. Lett. **79**, 5134-5137 (1997).

²² Y. Okimoto, T. Katsufuji, T. Ishikawa, A. Urushibara, T. Arima, and Y. Tokura Phys. Rev. Lett. **75**, 109-112 (1995).

²³ H.J.A. Molegraaf, C. Presura, D. van der Marel, P.H. Kes, and M. Li, Science **295**, 2239-2241 (2002).

²⁴ D. van der Marel, H.J.A. Molegraaf, J. Zaanen, Z. Nussinov, F. Carbone, A. Damascelli, H. Eisaki, M. Greven, P. H. Kes, and M. Li, Nature **425**, 271-274 (2003).

²⁵ A.B. Kuzmenko, N. Tombros, H.J.A. Molegraaf, M. Grüninger, D. van der Marel, and S. Uchida Phys. Rev. Lett. **91**, 037004 (2003)

²⁶ For details of the cryostat design see optics.unige.ch/vdm/marel_files/cryostat_design.htm

²⁷ H.J. Williams, J.H. Wernick, R.C. Sherwood, and G.K. Wertheim, J. Appl. Phys. **37**, 1256 (1966).

²⁸ S. Asanabe, D. Shinoda, and Y. Sasaki, Phys. Rev. **134**, A774-A779 (1964).

²⁹ Z. Schlesinger, Z. Fisk, H. T. Zhang, M. B. Maple, J. F. DiTusa, and G. Aeppli, Phys. Rev. Lett. **71**, 1748-1751 (1993).

³⁰ L. DeGiorgi, M. B. Hunt, H. R. Ott, M. Dressel, B.J. Feenstra, G. Grüner, Z. Fisk, and P. Canfield, Europhys. Lett. **28**, 341-346 (1994).

³¹ A. Damascelli, K. Schulte, D. van der Marel, and A.A. Menovsky, Phys. Rev. B **55**, R4863-R4866 (1997).

³² T. Jarlborg, Phys. Rev. B **59**, 15002 (1999).

³³ K. Urasaki, and T. Saso, Physica B **281-282**, 313-314 (1999).

³⁴ K. Urasaki, and T. Saso, Phys. Rev. B **58**, 15528-15533 (1998).

³⁵ M.J. Rozenberg, G. Kotliar, and H. Kajueter, Phys. Rev. B **54**, 8452-8468 (1996).

³⁶ C. Fu, M.P.C.M. Krijn, and S. Doniach, Phys. Rev. B **49**, R2219 (1994).

³⁷ M.A. Chernikov, L. Degiorgi, E. Felder, S. Paschen, A.D. Bianchi, H.R. Ott, J.L. Sarrao, Z. Fisk, and D. Mandrus Phys. Rev. B **56**, 1366-1375 (1997).

³⁸ F.P. Mena, *Ph D Thesis*, ISBN 90-367-2128-8, University of Groningen (2004); available on-line at www.ub.rug.nl/eldoc/dis/science/f.p.mena

³⁹ J. Guevara, V. Vildosola, J. Milano, and A.M. Llois Phys. Rev. B **69**, 184422 1-6 (2004).

⁴⁰ P.A. Wolff, Phys. Rev. **124**, 1030-1035, (1961).

⁴¹ A.M. Clogston, B.T. Matthias, M. Peter, H.J. Williams, E. Corenzwit, and R.C. Sherwood, Phys. Rev. **125**, 541552 (1962).

⁴² P.W. Anderson, Phys. Rev. **124**, 41-53 (1961).

⁴³ P.W. Anderson, Rev. Mod. Phys. **50**, 191-201 (1978).

⁴⁴ O. Gunnarsson, and B. Lundqvist, Phys. Rev. B **13**, 4274-4298 (1976).

⁴⁵ S.Y. Savrasov, and D.Y. Savrasov, Phys. Rev. B **46**, 12181-12195 (1992).

⁴⁶ I.I. Mazin, E. G. Maksimov, S.N. Rashkeev, S. Yu. Savrasov, and Yu.A. Uspenskii, JETP Letters **47**, 113-117 (1988).

⁴⁷ L.F. Mattheiss, D.R. Hamann, Phys. Rev. B **47**, 13114-13119 (1993).

⁴⁸ A. Fert, and A. Campbell, Phys. Rev. Lett. **21**, 1190 (1968).